IEEE Photonics Journal
An IEEE Photonics Society Publication

Reconfigurable Instantaneous Frequency Measurement System Based on Dual-Parallel Mach–Zehnder Modulator

Volume 4, Number 2, April 2012

Wei Li
Ning Hua Zhu, Member, IEEE
Li Xian Wang

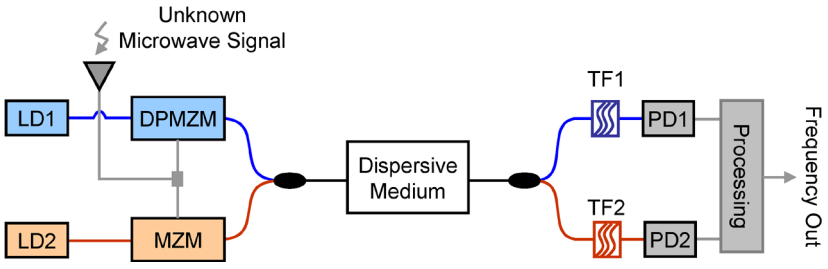

DOI: 10.1109/JPHOT.2012.2189102
1943-0655/$31.00 ©2012 IEEE

Reconfigurable Instantaneous Frequency Measurement System Based on Dual-Parallel Mach–Zehnder Modulator

Wei Li, Ning Hua Zhu, *Member, IEEE*, and Li Xian Wang

State Key Laboratory on Integrated Optoelectronics, Institute of Semiconductors, Chinese Academy of Sciences, Beijing 100083, China

DOI: 10.1109/JPHOT.2012.2189102
1943-0655/$31.00 ©2012 IEEE

Manuscript received January 29, 2012; accepted February 20, 2012. Date of publication February 27, 2012; date of current version March 15, 2012. This work was supported by the National Natural Science Foundation of China under 61108002, 61127018, 61021003, 61177060, 61090390, 61177080, and 60820106004. Corresponding author: W. Li (e-mail: liwei05@semi.ac.cn).

Abstract: We propose and demonstrate a novel reconfigurable instantaneous frequency measurement (IFM) system based on the dual-parallel Mach–Zehnder modulator (DPMZM). The IFM system can be reconfigurable with tunable measurement range and resolution by simply adjusting the dc bias voltage of the DPMZM. In principle, the measurement range could be tuned to any frequencies, which is only limited by the bandwidth of the optical transmitter and receiver employed. Alternatively, the IFM system can also work with a fixed wide measurement range and moderate resolution by generating two complementary power-fading functions.

Index Terms: Instantaneous frequency measurement (IFM), dual-parallel Mach–Zehnder modulator, (DPMZM).

1. Introduction

Modern electronic warfare and radar systems require a low latency tool for detecting and roughly classifying intercepted microwave signals. An instantaneous frequency measurement (IFM) system based on photonic techniques is a promising candidate [1]–[6]. Compared with conventional electronic techniques, the primary advantages of the photonic-assisted IFM are high bandwidth, low loss, light weight, and immunity to electromagnetic interference [7]–[9]. A number of techniques have been proposed for IFM systems [1]–[14]. In these schemes, generally, the frequency information of the unknown signals can be deduced by the frequency-to-space mapping [1]–[3], frequency-to-time mapping [4], and frequency-to-power mapping methods [5]–[13].

For the frequency-to-power mapping technique, a unique relationship between the microwave frequency and the measured optical power [5], [6] or electrical power [7]–[14] should be established. In [7], an amplitude comparison technique was proposed by comparing the two different dispersion-induced power-fading functions. However, the measurement errors are very large in the low-frequency range due to the flat amplitude comparison function (ACF). Therefore, the measurement range is basically restricted to the vicinity of the notch frequency. In this context, the amplitude comparison technique was improved to a wide measurement range by comparing two complementary power-fading functions using, for instance, a phase modulator plus an intensity modulator [8], a polarization modulator (PolM) [9], a polarization maintaining fiber (PMF) with a dispersion compensation fiber (DCF) [10], and a dual-electrode dual-output Mach–Zehnder modulator (MZM) [11].

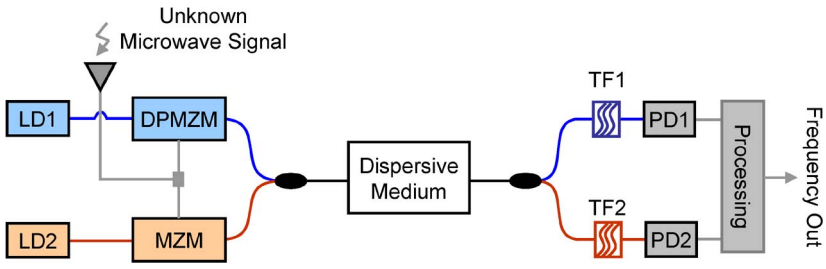

Fig. 1. Schematic configuration of the proposed IFM system (LD: laser diode; DPMZM: dual-parallel Mach–Zehnder modulator; TF: tunable optical filter; PD: photodetector).

The other limitation of the approach presented in [7] is the fixed measurement range and resolution. However, for many applications, it is highly desirable that the IFM system can be reconfigurable with adjustable measurement range and resolution. In [11]–[13], the reconfiguration of the IFM system was demonstrated by tuning the laser wavelength. The measurement range can only be adjusted in a narrowband due to the relative small dispersion variation resulting from the wavelength tuning. Recently, we have demonstrated a reconfigurable IFM system based on stimulated Brillouin scattering (SBS) [14]. However, the temperature control with high accuracy was required to guarantee the reported measurement resolution because the SBS is very sensitive to the environment. Moreover, the use of an additional frequency tunable electrical source (as well as the temperature control device) makes the system huge and expensive.

In this paper, we theoretically and experimentally demonstrate a novel reconfigurable IFM system based on dual-parallel MZM (DPMZM). Different from the previous wavelength tuning methods [11]–[13] and SBS-assisted approach [14], the IFM system is reconfigurable with tunable measurement range and resolution by simply adjusting the dc bias voltage of the DPMZM. In principle, the measurement range can be tuned to any frequencies, which is only limited by the bandwidth of the optical transmitter and receiver employed. Alternatively, the IFM system can also work with a fixed wide measurement range and moderate resolution by generating two complementary power-fading functions.

2. Principle

The schematic configuration of the proposed IFM system is shown in Fig. 1. The unknown microwave signal is modulated onto two independent optical carriers (OCs) with different wavelengths (λ_1 and λ_2) from two laser diodes (LD1 and LD2) using DPMZM and MZM, respectively. In our scheme, the wavelengths of the two LDs are fixed. In the lower channel, the MZM is biased at quadrature to generate a double sideband (DSB) modulated signal. The bias control of the DPMZM in the upper channel will be discussed later. These signals are then passed through a dispersive medium to induce two different power-fading functions. The dispersed signals are separated by two optical tunable filters (TF1 and TF2), detected by two photodetectors (PD1 and PD2, respectively). In this way, the ACF of the two power-fading functions can be constructed to realize frequency-to-power mapping. The power-fading function in the lower channel is fixed for a given IFM system. In order to tune the measurement range and resolution of the system, the power-fading function in the upper channel should be tunable.

The key component in our scheme is a commercially *x*-cut integrated DPMZM, also called differential quadrature phase-shift-keying (DQPSK) modulator. Fig. 2 illustrates the layout of the DPMZM, along with the schematic optical spectra at different locations. It is structured as two MZMs (MZM1 and MZM2) set in parallel and forming a third MZM (MZM3). In the DPMZM, MZM1 is fed by the unknown microwave signal and is biased at minimum transmission to implement carrier suppressed (CS)-DSB modulation. MZM2 has no driven signal and is biased at a maximum transmission point to allow the OC to pass through. They are combined together in MZM3 to generate

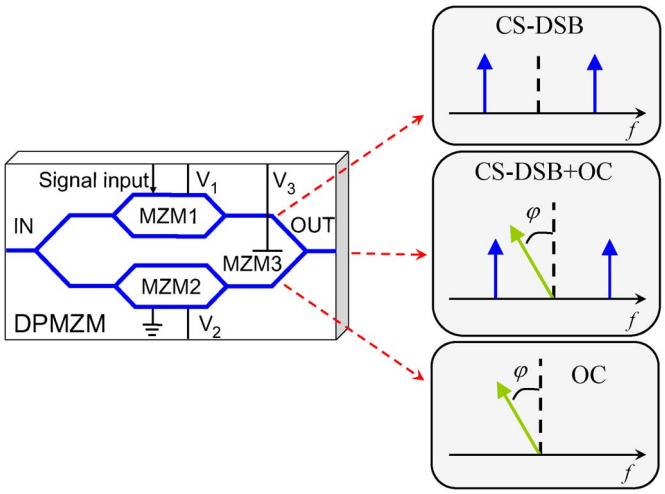

Fig. 2. Layout of the DPMZM, along with the schematic optical spectra at different locations.

a CS-DSB + OC signal. A frequency independent phase difference φ between the CS-DSB and OC signals is then generated by controlling the dc bias of MZM3, i.e., V_3. After passing through the dispersive medium, a frequency dependent phase shift is introduced to the CS-DSB signal with respect to the OC. This frequency-dependent phase shift results in the power-fading after photodetection. Note that the power-fading function, as well as the ACF, is tunable by adjusting the frequency-independent phase shift φ via tuning V_3. As a result, the IFM system is reconfigurable by simply adjusting the dc bias V_3. Next, the principle of the IFM system is investigated theoretically.

The optical field from the MZM1 is given by

$$E_1 = E_{\text{in}} \sin(\beta \cos 2\pi f_m t) \exp(j2\pi f_0 t)/\sqrt{2} \tag{1}$$

where V_{m} and f_{m} are the peak amplitude and frequency of the unknown microwave signal. $E_{\text{in}}\exp(j2\pi f_0 t)$ is the input optical field, f_0 is the frequency of the OC, $J_1(\beta)$ is the first-order Bessel function of the first kind, $\beta = \pi V_m/(2V_{\pi 1})$, and $V_{\pi 1}$ is the half-wave voltage of MZM1. Under small-signal conditions, only the first-order sidebands are considered and (1) can be simplified as

$$E_1 = \frac{E_{\text{in}}}{2\sqrt{2}} J_1(\beta) \exp[j2\pi(f_0 - f_m)t] + \frac{E_{\text{in}}}{2\sqrt{2}} J_1(\beta) \exp[j2\pi(f_0 + f_m)t]. \tag{2}$$

The optical field from MZM2 can be written by

$$E_2 = E_{\text{in}} \exp(j2\pi f_0 t)/\sqrt{2}. \tag{3}$$

After combination, the optical field from DPMZM can be expressed as

$$E_{\text{out1}} = [E_1 + E_2 \exp(j\varphi)]/\sqrt{2} \tag{4}$$

where $\varphi = \pi(V_3 - V_{\text{offset}})/V_{\pi 3}$ is the phase difference between CS-DSB and OC signals, $V_{\pi 3}$ is the half-wave voltage of MZM3, and V_{offset} is the offset voltage when $\varphi = 0$. After passing through a dispersive medium, the optical field is given by

$$E_{\text{out2}} = \frac{E_{\text{in}}}{4} J_1(\beta) \exp[j2\pi(f_0 - f_m)t] \exp\left(\frac{j\pi D_1 \lambda_1^2 f_m^2}{c}\right) + \frac{E_{\text{in}}}{2} \exp[j(2\pi f_0 t + \varphi)] + \frac{E_{\text{in}}}{4} J_1(\beta) \exp[j2\pi(f_0 + f_m)t] \exp\left(\frac{j\pi D_1 \lambda_1^2 f_m^2}{c}\right) \tag{5}$$

where D_1 is the total dispersion of the dispersive medium for λ_1. The microwave power after the PD is proportional to

$$P_m \propto J_1^2(\beta)\cos^2\left(\frac{\pi D_1\lambda_1^2 f_m^2}{c}-\varphi\right)=J_1^2(\beta)\cos^2\left[\frac{\pi D_1\lambda_1^2 f_m^2}{c}-\frac{\pi(V_3-V_{\text{offset}})}{V_{\pi 3}}\right]. \tag{6}$$

The difference between the two power-fading functions of the two channels (see Fig. 1), referred to as the ACF, is given by

$$\gamma=\eta\frac{J_1^2(\beta)\cos^2\left[\frac{\pi D_1\lambda_1^2 f_m^2}{c}-\frac{\pi(V_3-V_{\text{offset}})}{V_{\pi 3}}\right]}{J_0^2(\beta')J_1^2(\beta')\cos^2\left(\frac{\pi D_2\lambda_2^2 f_m^2}{c}\right)} \tag{7}$$

where D_2 is the total dispersion for λ_2, η is the power ratio coefficient, $\beta'=\pi V_{\text{m}}/(2V_\pi')$, and V_π' is the half-wave voltage of the MZM in the lower channel. Under small-signal conditions, i.e., $0<\beta$, $\beta'\ll 1$, we have $J_0(\beta')\sim 1$, $J_1(\beta)\sim\beta/2=\pi V_{\text{m}}/(4V_{\pi 1})$, and $J_1(\beta')\sim\beta'/2=\pi V_{\text{m}}/(4V_\pi')$. Then, (7) can be simplified as

$$\gamma=\eta'\frac{\cos^2\left[\frac{\pi D_1\lambda_1^2 f_m^2}{c}-\frac{\pi(V_3-V_{\text{offset}})}{V_{\pi 3}}\right]}{\cos^2\left(\frac{\pi D_2\lambda_2^2 f_m^2}{c}\right)} \tag{8}$$

where η' includes such as the losses in the dispersive medium, the modulator, the TF, and the PD. However, the loss difference between the two channels can be compensated by adjusting the optical power of the LDs. Therefore, we have $\eta'=1$. Then, (8) can be expressed as

$$\gamma=\frac{\cos^2\left[\frac{\pi D_1\lambda_1^2 f_m^2}{c}-\frac{\pi(V_3-V_{\text{offset}})}{V_{\pi 3}}\right]}{\cos^2\left(\frac{\pi D_2\lambda_2^2 f_m^2}{c}\right)}. \tag{9}$$

As can be seen from (9), a unique relationship between the input microwave frequency and power ratio is established. In this way, the input microwave frequency can be extracted from the measured ACF. Note that the ACF consists of two parts. One is the frequency dependent phase shift of the CS-DSB signal with respect to the OC, which leads to the powerfading. The other is the frequency independent phase shift φ, which is controlled by the dc bias V_3. In our scheme, all the parameters including the wavelengths of the two LDs and the total dispersion of the medium are fixed, except for V_3. The reconfiguration of the ACF can be simply accomplished by adjusting V_3. This is the key difference between the previous methods [11]–[13] and ours. In order to show the advantages of our method, the limitations of the conventional methods based on wavelength tuning are analyzed first.

When $V_3=V_{\text{offset}}$ $(\varphi=0)$, (9) is simplified as

$$\gamma=\frac{\cos^2\left(\pi D_1\lambda_1^2 f_m^2/c\right)}{\cos^2\left(\pi D_2\lambda_2^2 f_m^2/c\right)}. \tag{10}$$

It is the same as the conventional ACF [7], [12]. Fig. 3 shows the simulated results of the power-fading functions and the corresponding ACF in this case. As shown in Fig. 3(b), the variation of ACF is very small in the frequency range of 0 to ~50 GHz. Fig. 3(c) shows the calculated first-order derivative of the ACF. From 0 to ~50 GHz, the small variations of the ACF would result in large measurement error and frequency ambiguity. This, in turn, sets the lower measurement bound of the IFM system. It is expected that the measurement resolution near the notch frequency can be improved due to the distinct changes of the ACF in the vicinity of the notch, as shown in Fig. 3(c).

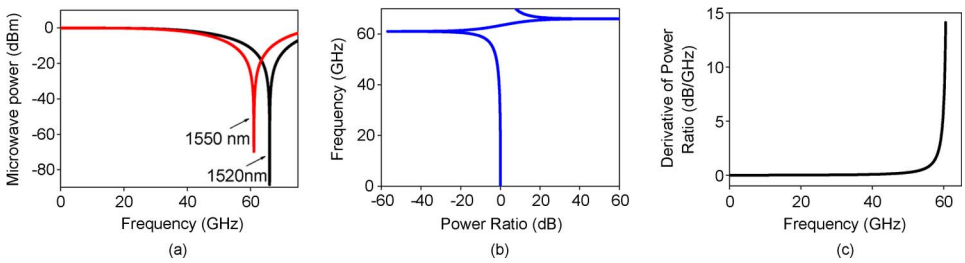

Fig. 3. Simulated results of (a) the power-fading functions, (b) the corresponding ACF, and (c) the calculated first-order derivative of the ACF for $V_3 = V_{\text{offset}}$ $(\varphi = 0)$ case. The parameters used in the simulation are $\lambda_1 = 1550$ nm, $\lambda_2 = 1520$ nm, $D_1 = 17$ ps/nm, and $D_2 = 14.9$ ps/nm.

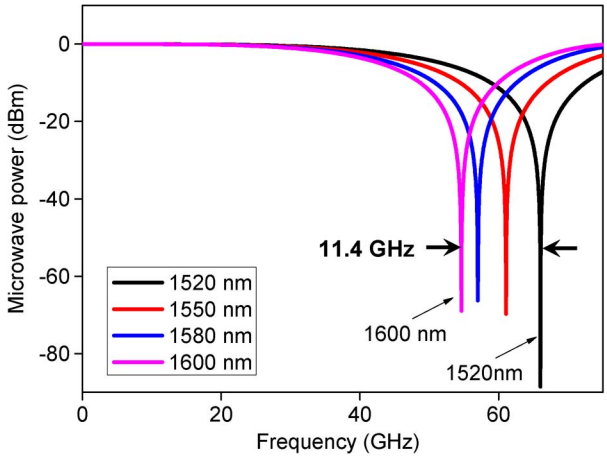

Fig. 4. Simulated power-fading functions when the wavelength is adjusted in the whole *C*-band. The parameters used in the simulation are $\lambda_1 = 1520$ nm $(D_1 = 14.9$ ps/nm), 1550 nm $(D_1 = 17$ ps/nm), 1580 nm $(D_1 = 18.4$ ps/nm), and 1600 nm $(D_1 = 19.7$ ps/nm).

In order to avoid frequency ambiguities, the upper measurement range of the IFM system is limited to the position of the first notch of the ACF, which is given by

$$M_{\max} = \sqrt{c/2D_1\lambda_1^2}. \tag{11}$$

In the conventional method, the measurement range is adjustable by tuning the wavelength of LD1 [12], as indicated by (11). Fig. 4 shows the simulated power-fading functions as the wavelength of LD1 is tuned. It can be seen that the first notch of the power-fading can only be adjusted in a frequency range as narrow as 11.4 GHz when the optical wavelength is tuned in the whole *C*-band. Therefore, the measurement range of the IFM system could only be tuned in a narrowband [12].

In our method, the reconfiguration of the system is accomplished by tuning the dc bias of the DPMZM V_3, while keeping the wavelengths of the two LDs unchanged. Fig. 5 shows the simulated power-fading functions when V_3 is tuned from 2.8 to 9.8 V. Note that the first notch of the power-fading is continuously tuned from around 0 to ~60 GHz. Fig. 6 shows the corresponding ACFs and the slopes of the ACFs. It is evident that the proposed system can be tuned in a much wider frequency range compared with the previous wavelength tuning methods [11]–[13]. Although the IFM system covers a wide frequency range, it is accomplished by tuning the dc bias V_3. In other words, for a fixed V_3, the measurement range is restricted around the frequency range over which the ACF varies sensibly.

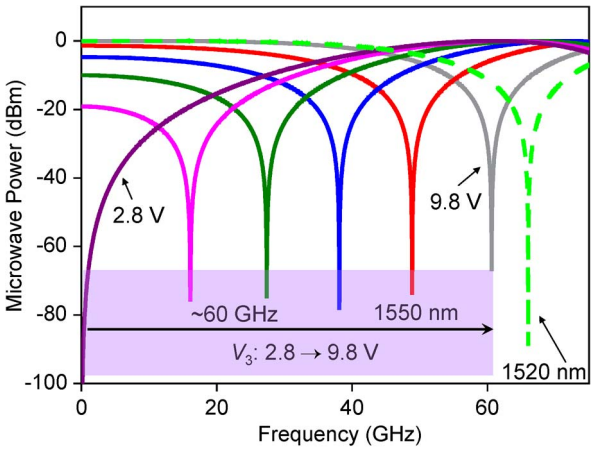

Fig. 5. Simulated power-fading functions when V_3 is tuned from 2.8 to 9.8 V.

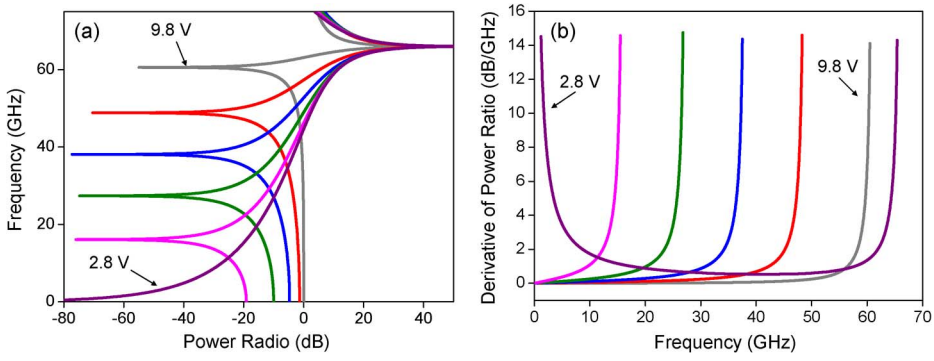

Fig. 6. (a) Calculated ACFs corresponding to Fig. 5 and (b) the first-order derivative of the ACFs. The parameters used in the simulation are $\lambda_1 = 1550$ nm, $\lambda_2 = 1520$ nm, $D_1 = 17$ ps/nm, and $D_2 = 14.9$ ps/nm, $V_{\pi 3} = 14$ V, and $V_{\text{offset}} = 9.8$ V. V_{offset} was measured by observing the maximum peak of the beating signal between OC and sidebands on the electrical spectrum analyzer (ESA) through the PD.

For $V_3 = 2.8$ V $(\varphi = \pi/2)$, (9) is simplified as

$$\gamma = \frac{\sin^2\left(\pi D_1 \lambda_1^2 f_m^2 / c\right)}{\cos^2\left(\pi D_2 \lambda_2^2 f_m^2 / c\right)}. \tag{12}$$

In this case, for the optical signal at λ_1, the intensity modulation at $V_3 = 9.8$ V (as shown in Fig. 5) is now converted to the phase modulation. As can be seen from Fig. 5, it generates power-fading functions that are bandpass (@ $\lambda_1 = 1550$ nm, $V_3 = 2.8$ V) and low-pass (@ $\lambda_2 = 1520$ nm), respectively. The complementary nature of the two power-fading functions leads to a fast change rate versus the input frequency over a wide range as shown in Fig. 6(b). It enables us to estimate the microwave frequency with a relative high resolution over a wide frequency range.

Note that $9.8 < V_3 < 11.1$ V should be avoided. In these cases, the notch @ $\lambda_1 = 1550$ will fall into the shadow area, as shown in Fig. 7. The power-fading @ λ_1 with $V_3 = 9.8$ V $(\varphi = 0)$ and that @ $\lambda_2 = 1520$ nm are also shown for reference. For $V_3 = 11.1$ V, the notch @ λ_1 locates at the same frequency as that of λ_2. A simulated example is shown in Fig. 7 with $V_3 = 10.74$ V. The zoom-in view shows that the two power-fading functions intersect at ~55.5 GHz. This intersection point dictates the lower bound of the IMF system, thus resulting in a very narrow measurement range.

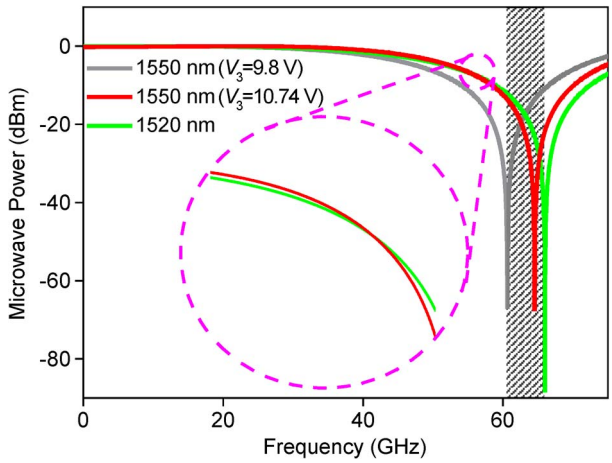

Fig. 7. Undesirable cases for the IFM system $(9.8 < V_3 < 11.1\ \text{V})$.

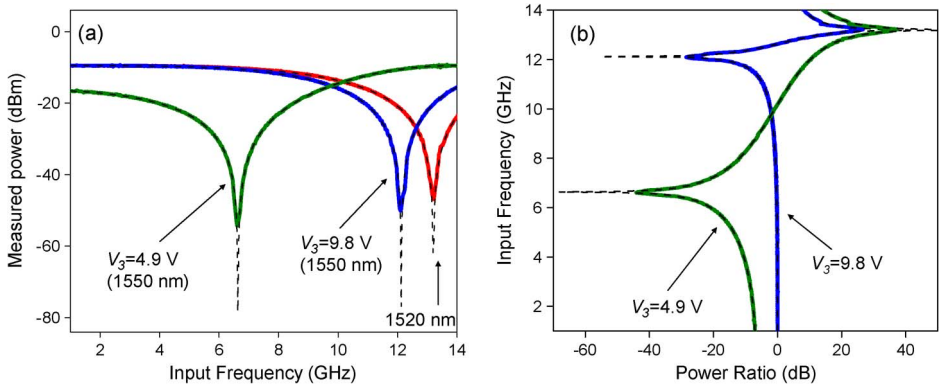

Fig. 8. Measured (solid lines) and simulated (dash lines) results of (a) power-fading functions and (b) ACFs for $V_3 = 4.9$ and 9.8 V, respectively.

For $V_3 = 2.8$ V, the upper measurement range is determined by the notch position @ λ_2 $(\lambda_1 > \lambda_2)$ [see Fig. 6(a)]. Therefore, the measurement range of the system is fixed in this case. For $2.8 < V_3 \leq 9.8$ V, the upper measurement range of the IFM system is determined by the notch @ λ_1 $(\lambda_1 > \lambda_2)$. The measurement range and resolution can be adjusted in this case. If the dispersive medium with smaller total dispersion is used, a higher upper measurement bound could be available. However, no matter how high the upper measurement bound is, a bias voltage tuning of 7 V (V_3, from 2.8 to 9.8 V) is enough to tune the notch of ACF [see Fig. 6(a)] through the whole frequency range. Therefore, in principle, the measurement range of the proposed IFM system can be tuned to any frequencies, which is only limited by the bandwidth of the optical transmitter and receiver employed.

3. Experiments

The most bandwidth-limiting components in our experiment are the PDs with 18 GHz bandwidth. Therefore, a 25-km S-SMF was used as the dispersive medium. The total dispersions for $\lambda_1 = 1550$ nm and $\lambda_2 = 1520$ nm were measured to be $D_1 = 425$ ps/nm and $D_2 = 372.5$ ps/nm, respectively, Fig. 8(a) shows the measured (solid lines) and simulated (dash lines) power-fading functions for the two channels (see Fig. 1). For the upper channel, the power-fading functions with $V_3 = 4.9$ and 9.8 V are shown. The power-fading functions were captured by a vector network

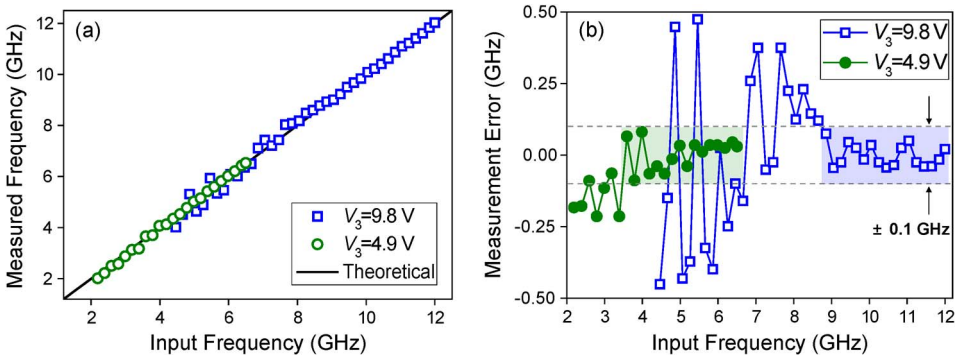

Fig. 9. (a) Measured frequency versus input frequency and (b) the measurement error as a function of input frequency for V3 = 4.9 and 9.8 V cases.

TABLE 1
Measurement range and resolution

V_3 (V)	Measurement range (GHz)	Resolution (GHz)
3.54	1–3.8	± 0.1
4.9	3.6–6.5	± 0.1
6.77	6.2–9	± 0.1
9.8	8.8–12	± 0.1

analyzer (VNA). The output power of the continuous-wave electrical signal from the VNA was set to -5 dBm. Fig. 8(b) shows the corresponding ACFs. Experimental results match well with the theoretical prediction. As shown in Fig. 8(a), the power-fading function at $\lambda_1 = 1550$ nm can be adjusted by tuning V_3. The variation of the first notch of the power-fading function influences the ACF and, finally, changes the upper measurement bound, as shown in Fig. 8(b).

Fig. 9 shows the measured frequency versus input frequency and the measurement error as a function of input frequency for $V_3 = 4.9$ and 9.8 V cases. It can be seen that the estimation of the input frequency is best closer to the notch of the ACF. At low frequencies, variations in the ACF are very small, leading to a large measurement error and frequency ambiguity. For a given measurement error, e.g., ± 0.1 GHz, the measurement range is tunable, as shown in Fig. 9(b). For $V_3 = 4.9$ and 9.8 V, the measurement range are 3.6–6.5 GHz and 8.8–12 GHz, respectively. Table 1 shows the measurement ranges and resolutions at different bias voltages. A total measurement range of 1–12 GHz with the resolution of ± 0.1 GHz was accomplished by tuning V_3. It should be noted that the total measurement range of 11 GHz is achieved by setting V_3 to four different bias voltages. For each working voltage, the measurement range is around 3 GHz.

Fig. 10 shows the measured (solid lines) and simulated (dash lines) power fading and the corresponding ACF for $V_3 = 2.8$ V $(\varphi = \pi/2)$ case. The complementary nature of the two power-fading functions leads to a relative fast change of the ACF versus the input frequency over a wide frequency range, as shown in Fig. 10(b). Fig. 11 shows the measured frequency as a function of the input frequency and the measurement error versus the input frequency. A measurement range as large as 11 GHz (2–13 GHz) was achieved for a moderate measurement resolution of ± 0.25 GHz.

4. Conclusion

We have demonstrated a reconfigurable IFM system based on DPMZM. The key component in our system is the DPMZM. In DPMZM, two sub-MZMs were biased at minimum and maximum transmission points, respectively, to generate a CS-DSB+OC modulated signal. In this way, a

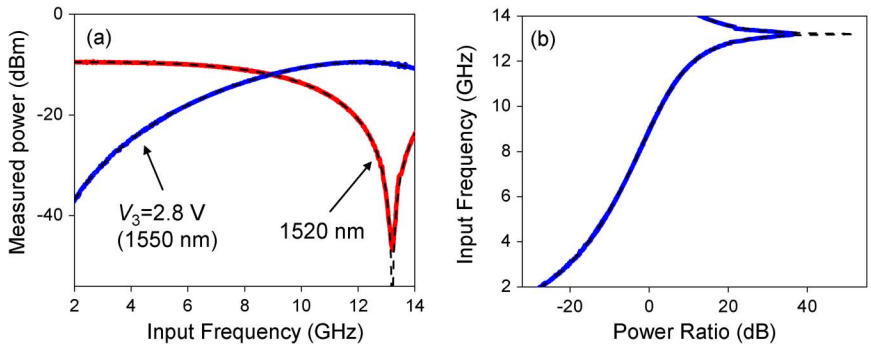

Fig. 10. Measured (solid lines) and simulated (dash lines) (a) power-fading functions and (b) the corresponding ACFs for $V_3 = 2.8$ V $(\varphi = \pi/2)$ case.

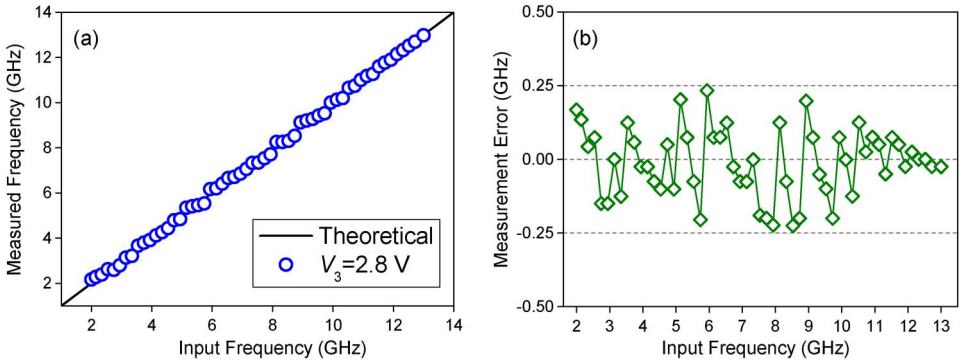

Fig. 11. (a) Measured frequency as a function of the input frequency and (b) the measurement error versus the input frequency for $V_3 = 2.8$ V $(\varphi = \pi/2)$ case.

phase-shift between the CS-DSB and OC signals was generated by controlling the dc bias of MZM3. This tunable phase-shift leads to an adjustable power-fading function, resulting in a tunable ACF. As a result, the IFM system is reconfigurable with tunable measurement range and resolution. In principle, the measurement range can be tuned to any frequencies, which is only limited by the bandwidth of the optical transmitter and receiver employed.

Compared with the previous methods based on wavelength tuning [11]–[13], the proposed method has two advantages: 1) The measurement range can be tuned in a much wider frequency range; 2) the system can also work with a fixed wide measurement range and moderate resolution. A proof-of-concept demonstration of the proposed technique has been presented. A total measurement range of 1–12 GHz with the resolution of $\pm$0.1 GHz has been achieved by tuning V_3 from 3.54 to 9.8 V. For $V_3 = 2.8$ V $(\varphi = \pi/2)$, a fixed measurement range as large as 11 GHz (2–13 GHz) has been accomplished with the resolution of $\pm$0.25 GHz. The maximum measurement bound in our experiment has been restricted by the limited bandwidth of PDs.

As indicated by (9), the ACF is determined by both the frequency dependent phase shift introduced by the dispersive medium and the frequency independent phase shift which is controlled by dc bias V_3. Therefore, the measurement errors can be attributed to such as the fluctuation of the optical source, the stability of the chromatic dispersion of the fiber, the stability of the bias control of the DPMZM, and the system noise. The frequency independent phase-shift φ changes with the bias voltage V_3, which results in the variation of ACF, leading to the measurement error. It can be seen from Fig. 6(a) that the variation of V_3 from 2.8 to 9.8 V is enough to tune the notch of the power-fading to any frequencies from around 0 to the maximum upper measurement bound. The

maximum upper measurement bound is inversely proportional to the total dispersion of the dispersive medium. For a larger tunable measurement range, the measurement error, however, is more sensitive to the fluctuation of V_3. Therefore, there is a tradeoff between the measurement range and resolution. The system shows an excellent short-term stability. However, due to the bias drifting of the modulator, the long-term stability of the system requires a more sophisticated voltage control.

References

[1] W. Wenshen, R. L. Davis, T. J. Jung, R. Lodenkamper, L. J. Lembo, J. C. Brock, and M. C. Wu, "Characterization of a coherent optical RF channelizer based on a diffraction grating," *IEEE Trans. Microw. Theory Tech.*, vol. 49, no. 10, pp. 1996–2001, Oct. 2001.

[2] D. B. Hunter, L. G. Edvell, and M. A. Englund, "Wideband microwave photonic channelised receiver," in *Proc. Int. Topical Meeting Microw. Photon.*, 2005, pp. 249–252.

[3] S. T. Winnall, A. C. Lindsay, M. W. Austin, J. Canning, and A. Mitchell, "A microwave channelizer and spectroscope based on an integrated optical Bragg-grating Fabry–Perot and integrated hybrid Fresnel lens system," *IEEE Trans. Microw. Theory Tech.*, vol. 54, no. 2, pp. 868–872, Feb. 2006.

[4] L. V. T. Nguyen, "Microwave photonic technique for frequency measurement of simultaneous signals," *IEEE Photon. Technol. Lett.*, vol. 21, no. 10, pp. 642–644, May 2009.

[5] X. Zou and J. P. Yao, "Microwave frequency measurement based on optical power monitoring using a complementary optical filter pair," *IEEE Trans. Microw. Theory Tech.*, vol. 57, no. 2, pp. 505–511, Feb. 2009.

[6] M. V. Drummond, P. Monteiro, and R. N. Nogueira, "Photonic RF instantaneous frequency measurement system by means of a polarization-domain interferometer," *Opt. Exp.*, vol. 17, no. 7, pp. 5433–5438, Mar. 2009.

[7] L. V. T. Nguyen and D. B. Hunter, "A photonic technique for microwave frequency measurement," *IEEE Photon. Technol. Lett.*, vol. 18, no. 10, pp. 1188–1190, May 2006.

[8] J. Zhou, S. Fu, S. Aditya, P. P. Shum, and C. Lin, "Instantaneous microwave frequency measurement using photonic technique," *IEEE Photon. Technol. Lett.*, vol. 21, no. 15, pp. 1069–1071, Aug. 2009.

[9] S. Pan and J. Yao, "Instantaneous microwave frequency measurement using a photonic microwave filter pair," *IEEE Photon. Technol. Lett.*, vol. 22, no. 19, pp. 1437–1439, Oct. 2010.

[10] J. Q. Zhou, S. Fu, P. P. Shum, S. Aditya, L. Xia, J. Li, X. Sun, and K. Xu, "Photonic measurement of microwave frequency based on phase modulation," *Opt. Exp.*, vol. 17, no. 9, pp. 7217–7221, Apr. 2009.

[11] J. Li, S. Fu, K. Xu, J. Q. Zhou, P. Shum, J. Wu, and J. Lin, "Photonic-assisted microwave frequency measurement with higher resolution and tunable range," *Opt. Lett.*, vol. 34, no. 6, pp. 743–745, Mar. 2009.

[12] X. Zou and J. Yao, "An optical approach to microwave frequency measurement with adjustable measurement range and resolution," *IEEE Photon. Technol. Lett.*, vol. 20, no. 23, pp. 1989–1991, Dec. 2008.

[13] X. Zhang, H. Chi, X. Zhang, S. Zheng, X. Jin, and J. Yao, "Instantaneous microwave frequency measurement using an optical phase modulator," *IEEE Microw. Wireless Compon. Lett.*, vol. 19, no. 6, pp. 422–424, Jun. 2009.

[14] W. Li, N. H. Zhu, and L. X. Wang, "Brillouin-assisted microwave frequency measurement with adjustable measurement range and resolution," *Opt. Lett.*, vol. 37, no. 2, pp. 166–168, Jan. 2012.